VESSEL EXTRACTION USING CROSSING-ADAPTIVE MINIMAL PATH MODEL WITH ANISOTROPIC ENHANCEMENT AND CURVATURE CONSTRAINT

Li Liu[1,2] *Da Chen*[2,3] *Laurent D. Cohen*[2] *Huazhong Shu*[1] *Michel Pagues*[3]

[1] Laboratory of Image Science and Technology, the Key Laboratory of Computer Network and Information Integration, Southeast University,210096 Nanjing, China
[2]Université Paris Dauphine, PSL Research University, CNRS, UMR 7534, CEREMADE, 75016 Paris, France
[3]Centre Hospitalier National dOphtalmologie des Quinze-Vingts, Paris, France

ABSTRACT

In this work, we propose a new minimal path model with a Riemannian metric updated scheme during the fast marching propagation for interactive vessel extraction. The invoked metric consists of a crossing-adaptive anisotropic radius-lifted tensor field and a front freezing indicator. The crossing-adaptive tensor field reduces the anisotropy of the metric on the crossing points. The indicator steers the front evolution by freezing the points causing high curvature of a geodesic. Thus the short branches combination problem commonly existing in tubular structure delineation by minimal path models can be solved. We validate our model on the DRIVE and IOSTAR datasets, which demonstrates that it is able to extract the centreline position and vessel width from a complex vessel network efficiently and accuracy.

Index Terms— Geodesic, anisotropy enhancement, Riemannian metric, path feature, tubular structure segmentation

1. INTRODUCTION

Vessel extraction is a crucial step in computer-assisted therapy applications [1]. The minimal path method is a suitable and efficient tool for vessel structure delineation, in which vessels are modelled as minimal paths associated to a metric. However, it is prone to short branches combination problem and an example is given in Fig. 1. A proper metric has essential importance in minimal path model, many improvements on which have been studied to address different situations in tubular structure segmentation.

The classic Eikonal PDE-based minimal path framework [2] proposes an isotropic Riemannian metric to measure the minimal path length, which delineates the vessel centerline. To further obtain the corresponding width of the vessel, the abstract radius variable is added to the image domain to construct the radius-lifted metric [3]. Recently, the anisotropic Riemannian metric taking into account the orientation information is widely studied to solve the short branches combination problem by the orientation enhancement [4, 5]. Besides, the curvature information is utilized to obtain a smooth minimal path such as the sub-Riemannian metric [6] and an Finsler elastica metric with curvature penalization [7].

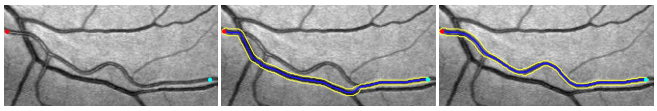

Fig. 1: Short branches combination problem. **Column 1** A retinal image patch with prescribed points (red and cyan dots). **Column 2** and **3** Minimal paths (blue curve) obtained from [4] and the proposed method, respectively. Yellow curve represents the vessel boundary.

Let $\Omega \subset \mathbb{R}^2$ be a 2-dimensional image domain. The multi-scale space is defined as $\bar{\Omega} := \Omega \times [r_{\mathrm{l}}, r_{\mathrm{h}}]$, where $[r_{\mathrm{l}}, r_{\mathrm{h}}]$ is the radius space. We denote by $\mathcal{S}_d^+$ the set of symmetric positive definite matrices with size of $d \times d\,(d = 2, 3)$ and let $\mathrm{Lips}([0,1], \bar{\Omega})$ be the set of Lipchitz continuous curves $\gamma : [0,1] \to \bar{\Omega}$. A minimal path is a curve $\gamma \in \mathrm{Lips}([0,1], \bar{\Omega})$ minimizing the path length $\mathfrak{L}$ globally measured through a radius-lifted anisotropic Riemannian metric $\mathcal{M} : \bar{\Omega} \to S_3^+$

$$\mathfrak{L}(\gamma) = \int_0^1 \sqrt{\gamma'(t)^{\mathrm{T}} \mathcal{M}(\gamma(t)) \gamma'(t)}\, dt. \tag{1}$$

where the metric $\mathcal{M}$ can be expressed as

$$\mathcal{M}(\bar{\mathbf{x}}) = \begin{pmatrix} \mathcal{M}_{\mathrm{a}}(\bar{\mathbf{x}}) & \mathbf{0} \\ \mathbf{0} & \mathcal{P}_{\mathrm{s}}(\bar{\mathbf{x}}) \end{pmatrix}, \tag{2}$$

where $\bar{\mathbf{x}} = (\mathbf{x}, r) \in \bar{\Omega}$, $\mathcal{M}_{\mathrm{a}} : \bar{\Omega} \to S_2^+$ is a tensor field associated to the spatial anisotropy and $\mathcal{P}_{\mathrm{s}} : \bar{\Omega} \to \mathbb{R}^+$ is a scalar function. Once the metric is determined, the minimal curve length between the source point $\bar{\mathbf{s}}$ and any point $\bar{\mathbf{x}}$ can be characterized by the geodesic distance map

$$\mathcal{U}_{\bar{\mathbf{s}}}(\bar{\mathbf{x}}) = \inf_{\gamma \in \mathrm{Lips}([0,1], \bar{\Omega})} \{\mathfrak{L}(\gamma); \gamma(0) = \bar{\mathbf{s}}, \gamma(1) = \bar{\mathbf{x}}\}, \tag{3}$$

which is the unique viscosity solution to the Eikonal PDE

$$\|\nabla \mathcal{U}_{\bar{\mathbf{s}}}(\bar{\mathbf{x}})\|_{\mathcal{M}^{-1}(\bar{\mathbf{x}})} = 1, \forall \bar{\mathbf{x}} \in \Omega \backslash \{\bar{\mathbf{s}}\}, \tag{4}$$

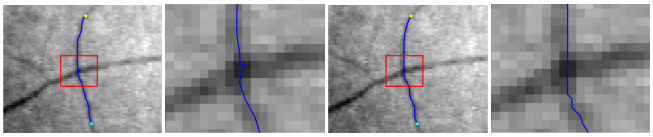

Fig. 2: Reducing the anisotropy of metric on crossing point. **Column 1** and **3** Minimal paths (blue curve) detected by [4] and the proposed crossing-adaptive metric, respectively. **Column 2** and **4** The region within the red rectangle. (Yellow and cyan points are prescribed.)

with $\mathcal{U}_{\bar{\mathbf{s}}}(\bar{\mathbf{s}}) = 0$. A geodesic $\hat{\mathcal{C}}_{\bar{\mathbf{x}},\bar{\mathbf{s}}}$ linking $\bar{\mathbf{x}}$ to $\bar{\mathbf{s}}$ can be tracked by solving the gradient descent ordinary differential equation (ODE):

$$\hat{\mathcal{C}}'_{\bar{\mathbf{x}},\bar{\mathbf{s}}}(t) = -\frac{\mathcal{M}^{-1}(\hat{\mathcal{C}}_{\bar{\mathbf{x}},\bar{\mathbf{s}}}(t))\nabla\mathcal{U}_{\bar{\mathbf{s}}}(\hat{\mathcal{C}}_{\bar{\mathbf{x}},\bar{\mathbf{s}}}(t))}{\|\mathcal{M}^{-1}(\hat{\mathcal{C}}_{\bar{\mathbf{x}},\bar{\mathbf{s}}}(t))\nabla\mathcal{U}_{\bar{\mathbf{s}}}(\hat{\mathcal{C}}_{\bar{\mathbf{x}},\bar{\mathbf{s}}}(t))\|}, \tag{5}$$

with $\hat{\mathcal{C}}_{\bar{\mathbf{x}},\bar{\mathbf{s}}}(0) = \bar{\mathbf{x}}$. The final geodesic $\mathcal{C}_{\bar{\mathbf{s}},\bar{\mathbf{x}}} \in \mathrm{Lips}([0,1],\bar{\Omega})$ can be obtained by reversing and reparameterizing $\hat{\mathcal{C}}_{\bar{\mathbf{x}},\bar{\mathbf{s}}}$.

In this work, we have proposed a dynamic anisotropic Riemannian metric depending on the geometric information and path feature in radius-lifted space, where the associated minimal paths favour to pass the vessel smooth.

2. THE NEW ANISOTROPIC GEODESIC METRIC WITH NONLOCAL INFORMATION

The main goal in this section is to establish a new Riemannian metric $\mathcal{M}_{\mathrm{d}}$ expressed by

$$\mathcal{M}_{\mathrm{d}}(\bar{\mathbf{x}}) = \mathcal{M}(\bar{\mathbf{x}})\delta(\bar{\mathbf{x}}), \forall(\bar{\mathbf{x}}) \in \bar{\Omega}. \tag{6}$$

It consists of two ingredients: the crossing-adaptive anisotropic radius-lifted tensor field $\mathcal{M} : \bar{\Omega} \to S_2^+$ and the front freezing indicator $\delta : \bar{\Omega} \to \{1, \infty\}$, which will be described in Sections 2.1 and 2.2.

2.1. Computation of the Crossing-Adaptive Tensor Field

We suppose that the intensities inside the tubular structures are lower than background. The crossing-adaptive tensor field $\mathcal{M}$ can be constructed by blocks as Eq. (2), which is based on an optimal direction $\mathbf{v}_1(\bar{\mathbf{x}})$ at each point $\bar{\mathbf{x}}$ and the corresponding eigenvalue λ_2 characterizing the appearance feature. The eigenvalues λ_i $(i = 1, 2, \cdots, d)$ extracted from the optimally oriented flux (OOF) filter [8] are the values of oriented flux along the corresponding eigenvectors $\mathbf{v}_i$, which are computed by $\lambda_i(\bar{\mathbf{x}}) = \mathbf{v}_i^T(\bar{\mathbf{x}})\,\mathbf{F}(\bar{\mathbf{x}})\mathbf{v}_i(\bar{\mathbf{x}})$. The optimal scale map $\eta : \Omega \to [r_1, r_{\mathrm{h}}]$ is defined to obtain the optimal direction and vesselness map by:

$$\eta(\mathbf{x}) = \underset{r\in[r_1,r_{\mathrm{h}}]}{\arg\max}\left\{\lambda_2(\mathbf{x}, r)\right\}. \tag{7}$$

We define the vesselness map $\zeta : \Omega \to \mathbb{R}_0^+$ and the tubular feature vector $\mathfrak{p} : \Omega \to \mathbb{R}^2$ at the optimal scale η:

$$\zeta(\mathbf{x}) = \max\left\{\lambda_2(\mathbf{x}, \eta(\mathbf{x})), 0\right\}, \mathfrak{p}(\mathbf{x}) = \mathbf{v}_1(\mathbf{x}, \eta(\mathbf{x})). \tag{8}$$

The short branches combination problem usually occurs at a crossing point due to the vector $\mathfrak{p}(\cdot)$ usually indicates the orientation of the stronger vessel at this crossing point. So the speed computed from the anisotropic metric is slower along the weak vessel than that along the strong one. To solve this problem, the anisotropy of the metric on a crossing point is reduced by utilizing the crossing-adaptive structure tensors as described [9]. The spatial anisotropy tensor filed $\mathcal{M}_{\mathrm{a}}$ and scalar function $\mathcal{P}_{\mathrm{s}}$ of $\mathcal{M}$ are shown as

$$\mathcal{M}_{\mathrm{a}}(\bar{\mathbf{x}}) = \exp(-\alpha\lambda_2(\bar{\mathbf{x}}))\mathcal{T}_{\mathrm{s}}(\bar{\mathbf{x}}), \mathcal{P}_{\mathrm{s}}(\bar{\mathbf{x}}) = \beta\exp(-\alpha\lambda_2(\bar{\mathbf{x}})). \tag{9}$$

where parameters $\alpha, \beta \in \mathbb{R}^+$ control the regularization of the spatial dimensions and radius dimension. The tensor field $\mathcal{T}_{\mathrm{s}} : \bar{\Omega} \to S_2^+$ is computed via a Gaussian kernel G_p with standard derivative p and the the identity matrix $\mathrm{I_d}$

$$\mathcal{T}_{\mathrm{s}}(\mathbf{x}, \cdot) = \Big((G_p * \mathcal{T})(\mathbf{x})/(G_p * \hbar)(\mathbf{x}) + \epsilon\,\mathrm{I_d}\Big)^{-1}, \tag{10}$$

where $\mathcal{T}(\mathbf{x}) = \hbar(\mathbf{x})\mathfrak{p}(\mathbf{x})\mathfrak{p}^T(\mathbf{x})$. The parameter $\epsilon \in \mathbb{R}^+$ is a sufficiently small constant to avoid the singularity, and $\hbar : \Omega \to \mathbb{R}_0^+$ is a weighted function to reduce the influence from the regions outside the vessel structures. We set $\hbar \cong \zeta$ (see in Eq. (8)) in this paper. If $\mathbf{x}$ is a vessel point and the vector $\mathfrak{p}$ changes slowly, then the eigenvector of the tensor $(G_p * \mathcal{T})(\mathbf{x})$, which corresponds to the largest eigenvalue, will approximate to the feature vector $\mathfrak{p}(\mathbf{x})$. For the vessel points $\mathbf{x}$ nearby a crossing structure, the feature vectors potentially vary fast, leading to that the tensors $(G_p * \mathcal{T})(\mathbf{x})$ are nearly isotropic. In Fig. 2, we illustrate the effect to remove the anisotropy of the metric in crossing point.

2.2. Computation of the Front-Freezing Indicator

The front-freezing indicator $\delta(\bar{\mathbf{x}})$ is computed based on the path feature derived from the curvature of the local geodesic through two extra points $\bar{\mathbf{m}}$, $\bar{\mathbf{z}}$ located on it like the method in [10]. The local geodesic can be computed through solving the gradient descent ODE (see in Eq. (5)) on the obtained geodesic distance map. Let $|\mathcal{C}|$ denote the geodesic length. Backtracking from $\bar{\mathbf{x}}$ stops when $|\mathcal{C}_{\bar{\mathbf{x}},\bar{\mathbf{z}}}| = \Gamma$, where Γ is a constant and $\bar{\mathbf{z}}$ is the back-tracked truncated point. The point $\bar{\mathbf{m}}$ is another extra point defined as the middle point along the local geodesic. The curvature $\mathcal{K}$ is measured by the angle between two vectors from the local geodesic as in [11] as:

$$\mathcal{K}(\bar{\mathbf{x}}) = \langle(\bar{\mathbf{m}}-\bar{\mathbf{z}}), (\bar{\mathbf{x}}-\bar{\mathbf{m}})\rangle/(\parallel \bar{\mathbf{m}}-\bar{\mathbf{z}} \parallel \times \parallel \bar{\mathbf{x}}-\bar{\mathbf{m}} \parallel), \tag{11}$$

where $\langle\cdot,\cdot\rangle$ denotes scalar product, $||\cdot||$ represents the norm of the vector. The range of $\mathcal{K}$ is $[1, -1]$.

The indicator δ is constructed to determine the curvature range of the tubular structure.

$$\delta(\bar{\mathbf{x}}) = \begin{cases} 1 & \mathcal{K}(\bar{\mathbf{x}}) > \mathcal{K}_0 \\ +\infty & \text{otherwise} \end{cases}, \tag{12}$$

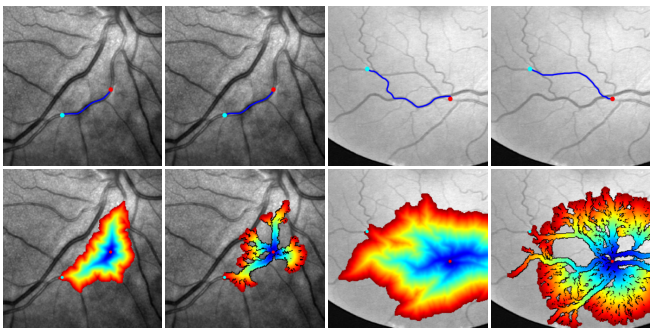

Fig. 3: **Raw 1** Retinal image patches with minimal path (blue curve) and prescribed points (red and cyan dots). **Raw 2** Geodesic distances superimposed on the original images. **Column 1** and **3** are computed from [4]. **Column 2** and **4** are obtained by the proposed model (Frozen points are denoted as black dots.).

where $\mathcal{K}_0$ is a given threshold. If the value of $\mathcal{K}$ for the current point is bigger than the given threshold, the wavefront is propagated as usual, otherwise the this point is frozen. The indicator takes into account the curvature constraint in order to seek geodesics without sharp turnings. Such an indicator is motivated by the fact that the retina blood vessels usually appear as linear structures with low curvatures. As an example, we show the frozen points violating the criterion as black points in columns 2 and 4 of Fig. 3.

Algorithm 1 Fast Marching Method

Output: Minimal action map $\mathcal{U}_{\mathrm{s}}$.
Initialization: Set $\forall \bar{\mathbf{x}} = (\mathbf{x}, r) \in \bar{\Omega} \setminus \{\bar{\mathbf{s}}\}$, set $\mathcal{U}_{\bar{\mathbf{s}}}(\bar{\mathbf{x}}) \leftarrow \infty$, $\mathcal{L}(\bar{\mathbf{x}}) \leftarrow Far$; $\mathcal{U}_{\bar{\mathbf{s}}}(\bar{\mathbf{s}}) \leftarrow 0$, $\mathcal{L}(\bar{\mathbf{s}}) \leftarrow Trial$; $\mathcal{F}(\mathbf{x}) \leftarrow 0$.

```
while stopping criterion is not reached do
    Find x̄_m minimizing U_s̄ and set L(x̄_m) ← Accepted;
    if F(x_m) = 0 then
        Compute curvature K via Eq. (11);
        if K ≤ K_0 then
            Set U_s̄(x̄_m) ← ∞ and F(x_m) ← 1;
        else
            for all ȳ ∈ H(x̄_m) and L(ȳ) ≠ Accepted do
                Set L(ȳ) ← Trial and compute U_s̄(ȳ);
            end for
        end if
    else
        Set U_s̄(x̄_m) ← ∞;
    end if
end while
```

3. FAST MARCHING IMPLEMENTATION

In the course of fast marching front propagation, all the grid points are labeled as three classes: Far, $Trial$ and $Accepted$. The geodesic distance is estimated by solving the Hopf-Lax operator defined in [12]. The stencil $\mathcal{N}(\bar{\mathbf{x}})$ determines the neighbourhood for each point $\bar{\mathbf{x}}$, and its inverse neighbourhood can be described as $\mathcal{H}(\bar{\mathbf{x}}) := \{\bar{\mathbf{y}} \in \mathbb{Z}^3; \bar{\mathbf{x}} \in \mathcal{N}(\bar{\mathbf{y}})\}$. The procedure for the fast marching method is described in Algorithm. 1.

The proposed Riemannian tensor field $\mathcal{M}_{\mathrm{d}}$ is updated during the geodesic distance computation which is actually carried out by computing the front-freezing indicator in a fronts advancing procedure to determine whether the front points should be frozen or not. In implementation, once a point $(\mathbf{x}, r)$ is frozen, all the points at position $\mathbf{x}$ with different radius scale belonging to $[r_{\mathrm{l}}, r_{\mathrm{h}}]$ will be frozen and tagged as $Accepted$. This scheme is helpful to save calculation consuming. It is achieved by defining a flag map $\mathcal{F} : \Omega \to \{0, 1\}$, where $\mathcal{F}(\mathbf{x}) = 1$ denotes that the point at position $\mathbf{x}$ is frozen. During fast marching fronts propagation, once the point $(\mathbf{x}, r)$ with minimal geodesic on the front is chosen, the value of $\mathcal{F}(\mathbf{x})$ can be checked.

For better visualization, we consider a new distance map $\mathcal{U}^*_{\bar{\mathbf{s}}}$ obtained by minimzing $\mathcal{U}_{\bar{\mathbf{s}}}$ over the last dimension

$$\mathcal{U}^*_{\bar{\mathbf{s}}}(\mathbf{x}) = \min_{r \in [r_{\mathrm{l}}, r_{\mathrm{h}}]} \{\mathcal{U}_{\bar{\mathbf{s}}}(\mathbf{x}, r)\} \tag{13}$$

In Fig. 3, we show two examples for $\mathcal{U}^*_{\bar{\mathbf{s}}}$.

4. EXPERIMENTAL RESULTS AND DISCUSSION

In this section, we evaluated our proposed model on retinal image patches from the DRIVE[11] and IOSTAR[13] datasets quantitatively and qualitatively. An measurement operator $\mathcal{R}$ is defined to validate the segmentation result quantitatively. Let $\mathcal{S}$ represent the pixel set of the segment result and $\mathcal{G}$ denotes the ground truth set. In addition, $\#\|\cdot\|$ denotes the number of pixels within the set. Thus the measurement is defined as:$\mathcal{R} = \#\|\mathcal{S} \cap \mathcal{G}\|/\#\|\mathcal{S}\|$, where $\mathcal{R} \in [0, 1]$. $\mathcal{R} = 1$ means that the segmented result is exactly same with the ground truth. We compare our proposed crossing-adaptive anisotropic radius-lifted tensor field $\mathcal{M}$ (caArR), the dynamic Riemannian metric $\mathcal{M}_{\mathrm{d}}$ (dArR) with the anisotropic radius-lifted Riemannian metric (ArR)[4].

Dataset		ArR	caArR	dArR
DRIVE	Avg.	0.365	0.580	0.861
	Std.	0.238	0.296	0.041
IOSTAR	Avg.	0.790	0.815	0.881
	Std.	0.237	0.210	0.193

Table 1: Quantitative comparison results on retinal images.

We consider $\Gamma = 8$ and $\mathcal{K}_0 = 0.9$ reasonable choice for the experiment. Besides, the parameter $\epsilon = 0.05$ is used to determine the anisotropic property of the structure tensor. The parameter $\alpha = 5$ is related to the influence of the appearance features. The parameter $\beta = 0.5$ controls the radius speed.

We compare the caArR metric with the classic ArR metric on retinal image patches, which are illustrated in Fig. 4. We

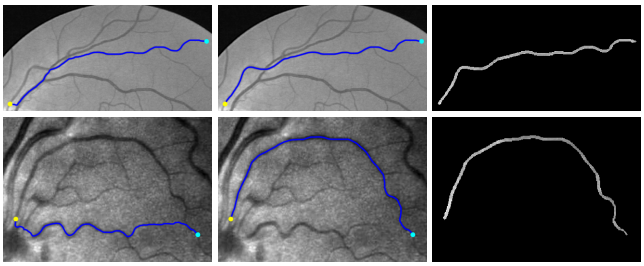

Fig. 4: Comparison results on retinal images. **Column 1**and **2** Minimal paths (blue curve) detected by [4] and the proposed crossing-adaptive metric, respectively. **Column 3** Vessel with thickness. Cyan and yellow dote are prescribed.

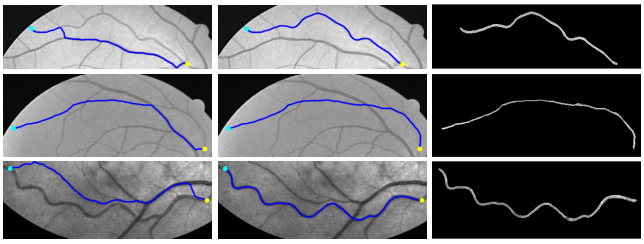

Fig. 5: Comparison results on retinal images. **Column 1**and **2** Minimal paths (blue curve) detected by [4] and the proposed model, respectively. **Column 3** Vessel with thickness. Cyan and yellow dote are predefined.

show the comparison result of the dArR with the ArR metric in Fig. 5. Besides, the quantitative evaluation is computed by the measurement operator $\mathcal{R}$ shown in Table. 1. We observe that the classic ArR metric suffered from short branches combination problem in some situations. The caArR metric and dArR metric can get the desired geodesic by reducing the anisotropy in the crossing section and take into account the curvature feature.

5. CONCLUSION

In this paper, we have proposed a new minimal path model with dynamic Riemannian metric for tubular structure segmentation by integrating the local geometric feature and non-local path feature. We constructed the dynamic Riemannian metric during the fast marching front propagation. The quantitative and qualitative results demonstrated that our method indeed solves the short branches combination problem in some situations and detects the desired vessel region from complex background.

6. REFERENCES

[1] C. Kirbas and F. Quek, "A review of vessel extraction techniques and algorithms," *ACM Computing Surveys*, vol. 36, no. 2, pp. 81–121, 2004.

[2] L.D. Cohen and R. Kimmel, "Global minimum for active contour models: A minimal path approach," *IJCV*, vol. 24, no. 1, pp. 57–78, 1997.

[3] H. Li and A. Yezzi, "Vessels as 4-d curves: Global minimal 4-d paths to extract 3-d tubular surfaces and centerlines," *TMI*, vol. 26, no. 9, pp. 1213–1223, 2007.

[4] F. Benmansour et al., "Tubular structure segmentation based on minimal path method and anisotropic enhancement," *IJCV*, vol. 92, no. 2, pp. 192–210, 2011.

[5] S. Bougleux et al., "Anisotropic geodesics for perceptual grouping and domain meshing," in *ECCV*. Springer, 2008, pp. 129–142.

[6] E.J. Bekkers et al., "A pde approach to data-driven sub-riemannian geodesics in se (2)," *SIAM*, vol. 8, no. 4, pp. 2740–2770, 2015.

[7] D. Chen et al., "Global minimum for a finsler elastica minimal path approach," *IJCV*, vol. 122, no. 3, pp. 458–483, 2017.

[8] M. Law and A.C. Chung, "Three dimensional curvilinear structure detection using optimally oriented flux," in *ECCV*. Springer, 2008, pp. 368–382.

[9] M. Law et al., "Gradient competition anisotropy for centerline extraction and segmentation of spinal cords," in *IPMI*. Springer, 2013, pp. 49–61.

[10] W. Liao et al., "Progressive minimal path method for segmentation of 2d and 3d line structures," *PAMI*, vol. 40, no. 3, pp. 696–709, 2018.

[11] A Qureshi et al., "A bayesian framework for the local configuration of retinal junctions," in *CVPR*, 2014, pp. 3105–3110.

[12] J. Mirebeau, "Anisotropic fast-marching on cartesian grids using lattice basis reduction," *SIAM*, vol. 52, no. 4, pp. 1573–1599, 2014.

[13] J. Zhang et al., "Robust retinal vessel segmentation via locally adaptive derivative frames in orientation scores," *TMI*, vol. 35, no. 12, pp. 2631–2644, 2016.